Assembly of Tetrameric Dimethyltin-Functionalized Selenotungstates: From Nanoclusters to One-Dimensional Chains

Wei-Chao Chen,[a] Chao Qin,[a] Yang-Guang Li,[a] Hong-Ying Zang,[a] Kui-Zhan Shao,[a] Zhong-Min Su,*[a] En-Bo Wang[a] and Hong-Sheng Liu*[b]*

[a]*Institute of Functional Material Chemistry, Key Lab of Polyoxometalate Science of Ministry of Education, Faculty of Chemistry, Northeast Normal University, Changchun, 130024 Jilin, People's Republic of China.*
[b]*School of Chemistry and Chemical Engineering, Daqing Normal University; Key Laboratory of Oilfield Applied chemistry, College of Heilongjiang Province, Daqing 163712, People's Republic of China.*

CONTENTS

Section 1 A Detailed Survey of Dimethyltin-Containing POMs

Table S1. A detailed survey of dimethyltin-containing POMs

Year	Formula	Basic Building Blocks	Number of Sn Centers	Dimension	Ref.
2004	$(CsNa_2[\{Sn(CH_3)_2\}_3(H_2O)_4(\beta\text{-}XW_9O_{33})]\cdot 7H_2O)_\infty$ (X = As, Sb)	Keggin-type $\{XW_9O_{33}\}$ (X = As, Sb)	3	2D lattice	1
2005	$[\{Sn(CH_3)_2(H_2O)\}_2\{Sn(CH_3)_2\}As_3(\alpha\text{-}AsW_9O_{33})_4]^{21-}$	Keggin-type $\{AsW_9O_{33}\}$	3	0D nanocluster	2
2005	$[\{SnCH_3)_2(H_2O)\}_{24}\{Sn(CH_3)_2\}_{12}(A\text{-}XW_9O_{34})_{12}]^{36-}$ (X = P, As)	Keggin-type $\{XW_9O_{34}\}$ (X = P, As)	36	0D nanocluster	3
2006	$[\{Sn(CH_3)_2\}_4(H_2P_4W_{24}O_{92})_2]^{28-}$	Dawson-type $\{H_2P_4W_{24}O_{92}\}$	4	0D nanocluster	4
2006	$[\{(CH_3)_2Sn\}(MoO_4)]$ (**1**) $[\{(CH_3)_2Sn\}_4O_2(MoO_4)_2]$ (**2**) $[\{(CH_3)_2Sn\}\{Mo_2O_7(H_2O)_2\}]\cdot H_2O$ (**3**)	$\{MoO_4\}$ $\{MoO_4\}$ $\{Mo_2O_7(H_2O)_2\}$	1 4 1	3D network 2D layer 2D layer	5
2006	$[\{(CH_3)_2Sn\}_2(W_6O_{22})]^{4-}$	$\{W_6O_{22}\}$	2	1D chain	6
2007	$[\{(Sn(CH_3)_2)(Sn(CH_3)_2O)(A\text{-}PW_9O_{34})\}_3]^{21-}$	Keggin-type $\{PW_9O_{34}\}$	6	0D nanocluster	7
2007	$[\{(CH_3)_2Sn\}_6(OH)_2O_2(H_2BW_{13}O_{46})_2]^{12-}$	Keggin-type $\{H_2BW_{13}O_{46}\}$	6	0D nanocluster	8
2008	$[\{(CH_3)_2Sn(H_2O)\}_4\{(CH_3)_2Sn\}(B\text{-}\beta\text{-}XW_9O_{33})_2]^{8-}$ (X = As, Sb)	Keggin-type $\{XW_9O_{33}\}$ (X = As, Sb)	5	2D assemblies	9
2009	$Na[C(NH_2)_3]_2[\{(CH_3)_2Sn(H_2O)\}_3(A\text{-}\alpha\text{-}PW_9O_{34})]\cdot 9H_2O$ (**1**) $Na[C(NH_2)_3]_2[\{(CH_3)_2Sn(H_2O)\}_3\text{-}(A\text{-}\alpha\text{-}AsW_9O_{34})]\cdot 8H_2O$ (**2**) $Na_2[C(NH_2)_3]_2[\{(CH_3)_2Sn(H_2O)\}_3(A\text{-}\alpha\text{-}SiW_9O_{34})]\cdot 10H_2O$ (**3**)	Keggin-type $\{XW_9O_{34}\}$ (X = P, As, Si)	3	3D networks	10
2010	$[\{(CH_3)_2Sn(H_2O)\}\{(CH_3)_2Sn\}(A\text{-}\alpha\text{-}PW_9O_{34})]^{5-}$ (**1**) $[\{(CH_3)_2Sn(H_2O)_2\}\{(CH_3)_2Sn(H_2O)\}_2(A\text{-}\alpha\text{-}PW_9O_{34})]^{3-}$ (**2**)	Keggin-type $\{PW_9O_{34}\}$	2 3	1D chain 2D assembly	11

	$[\{(CH_3)_2Sn(H_2O)\}_3(A\text{-}\alpha\text{-}PW_9O_{34})]^{3-}$ (**3**)		3	3D network	
2014	$(C_2H_8N)_7Na_{12}[\{Sn(CH_3)_2\}_4\{Sn(CH_3)_2(H_2O)\}_2\{Sn(CH_3)_2(H_2O)_2\}Se_8W_{54}O_{191}(OH)_7(H_2O)_2]\cdot 64H_2O$ (**1**) $(C_2H_8N)_8Na_{10}[\{Sn(CH_3)_2\}_{10}\{Sn(CH_3)_2(H_2O)\}_6Se_{11}W_{56}O_{211}(OH)_8]\cdot 105H_2O$ (**2**)	$\{Se_4W_{27}\}$ & Dawson-type $\{Se_2W_{12}\}$ and $\{\beta\text{–}Se_2W_{15}\}$ Dawson-type $\{\gamma\text{–}Se_2W_{14}\}$	7 16	0D nanocluster chain	this work

References：

[1] F. Hussain, M. Reicke and U. Kortz, *Eur. J. Inorg. Chem.*, 2004, 2733–2738.

[2] F. Hussain and U. Kortz, *Chem. Commun.*, 2005, 1191–1193.

[3] U. Kortz, F. Hussain and M. Reicke, *Angew. Chem., Int. Ed.,* 2005, **44**, 3773–3777.

[4] F. Hussain, U. Kortz, B. Keita, L. Nadjo and M. T. Pope, *Inorg. Chem.*, 2006, **45**, 761–766.

[5] S. Reinoso, M. H. Dickman, M. Reicke and U. Kortz, *Inorg. Chem.*, 2006, **45**, 9014–9019.

[6] S. Reinoso, M. H. Dickman and U. Kortz, *Inorg. Chem.*, 2006, **45**, 10422–10424.

[7] F. Hussain, M. H. Dickman, U. Kortz, B. Keita, L. Nadjo, G. A. Khitrov and A. G. Marshall, *J. Cluster Sci.*, 2007, **18**, 173–191.

[8] S. Reinoso, M. H. Dickman, M. F. Matei and U. Kortz, *Inorg. Chem.*, 2007, **46**, 4383–4385.

[9] S. Reinoso, M. H. Dickman and U. Kortz, *Eur. J. Inorg. Chem.*, 2009, 947–953.

[10] L. F. Piedra-Garza, S. Reinoso, M. H. Dickman, M. M. Sanguineti and U. Kortz, *Dalton Trans.*, 2009, 6231–6234.

[11] S. Reinoso, B. S. Bassil, M. Barsukova and U. Kortz, *Eur. J. Inorg. Chem.*, 2010, 2537–2542.

Section 2 Synthesis, Crystal Data, and Structures of 1-2

2.1 Synthesis

Materials: All chemicals and solvents were commercially purchased and used without further purification.

Synthesis of 1: $Na_2WO_4{\cdot}2H_2O$ (1.70 g, 5.12 mmol) and Na_2SeO_3 (0.13 g, 0.73 mmol) were dissolved in 30 mL water. The pH value of the solution was adjusted to 5.0 by the 50% (1:1) acetic acid solution. After the solution was stirred for around 30 min, solid $(CH_3)_2SnCl_2$ (0.40 g, 1.82 mmol) and dimethylamine hydrochloride (0.70 g, 6.13 mmol) were successively added. The final pH was kept at 3.5 by 2 M HCl. This solution was stirred for another 10 min and then heated to 80 ^oC stirred for 1 h, cooled down to room temperature, filtered and left to evaporate slowly. Colorless block-shaped crystals were obtained after three weeks, which were then collected by filtration and air-dried. Yield: 0.37 g, (23.4 %, based on W). IR (in cm^{-1}): 3421 (w), 3107 (w), 2779 (w), 1626 (w), 1468 (s), 1413 (m), 1198 (w), 1025 (m), 946 (s), 841 (w), 742 (w). Elemental analysis, calc. for $C_{28}H_{245}N_7Na_{12}O_{268}Se_8Sn_7W_{54}$: C 2.02, N 0.59, Na 1.66, Sn 5.00, Se 4.46, W 59.7 %; Found C 2.16, N 0.44, Na 1.51, Sn 5.21, Se 4.27, W 57.3 %.

Synthesis of 2: The synthesis process of **2** is similar to **1**, but the pH of the solution was adjusted to 4.8 by the addition of aqueous 2 M HCl before heating to 80 °C. Slow evaporation of the solution results in the colorless needle-shaped crystals **2** forming in one month. Yield: 0.20 g, (11.2 %, based on W). IR (in cm^{-1}): 3436 (w), 3108 (w), 2792 (w), 1621 (s), 1471 (s), 1410 (m), 1199 (w), 1021 (m), 960 (s), 844 (m), 769 (w). Elemental analysis, calc. for $C_{48}H_{390}N_8Na_{10}O_{330}Se_{11}Sn_{16}W_{56}$: C 2.93, N 0.57, Na 1.17, Sn 9.66, Se 4.42, W 52.4 %; Found C 2.61, N 0.74, Na 1.31, Sn 9.43, Se 4.60, W 50.3 %.

2.2 Synthesis Discussion

The precise control of the one−pot reaction conditions of combining $(CH_3)_2Sn^{2+}$ groups with the SeO_3^{2-} anion templates at proper pH was employed for the assembly of **1**−**2**. Since the SeO_3^{2-} anion templates have a lone pair of electrons and only form three bonds through oxygen atoms in trigonal configurations, they effectively give rise to "open" lacunary units instead of "closed" Wells−Dawson−type clusters, owing to the inducing effect of the lone pair of electrons. Such templates can also be viewed as "inorganic ligands" as well as linkers according to previous reports.[1] Moreover, the electrophile $(CH_3)_2Sn^{2+}$ groups possess the stability of the Sn−C bond in aqueous media and also the fact that Sn^{IV} can substitute for addenda metals in POM skeletons[2]. Significantly, *trans*− or *cis*−$(CH_3)_2Sn^{2+}$ moieties realize that dimethyltin−containing POMs develop abundant architectures, especially from discrete assemblies to extended polyanion−based materials[2]. Therefore, a synergistic effect between $(CH_3)_2Sn^{2+}$ groups and the anion template effect of SeO_3^{2-} may guide the construction of unprecedented dimethyltin−functionalized selenotungstates.

First, we chose Na_2WO_4 and Na_2SeO_3 as the W− & Se−sources. The acidification of them (W/Se molar ratio 7:1) by acetic acid was necessary.[1] Acetic acid has already been proven to be a suitable reagent for acidifying Se−based POTs clusters[1b,1i], and furthermore, the molar ratio also plays an important role that is in accordance with the final structures: such as the $\{Se_4W_{27}\}$ fragments in **1** (W:Se molar ratio 7:1) and the Wells−Dawson−type $\{\gamma$–$Se_2W_{14}\}$ building blocks in **2** (W:Se molar ratio 7:1).

Subsequently, dimethyltin species ($(CH_3)_2Sn^{2+}$) and organic amine salts were introduced to the acid solution. Among several factors (e.g., reaction solvents and temperature) during the synthesis, the features of the countercation constitute a key factor in the formation of several POMs, and therefore, choosing desirable counteraction may allow for a rational design of tailored POM assemblies[2a]. Recently, Kortz et al. demonstrated that the $[C(NH_2)_3]^+$ cation can be used as a structure–directing agent to construct supramolecular arrangements, especially for dimethyltin–containing POMs[2j,2k], as a result of its rigid and planar geometry and its hydrogen

bonding capability over a wide pH range. In this context, Cronin et al. has also investigated the templating effect of some organo–ammonium cations, such as $[C_2H_8N]^+$, in the construction of novel POM frameworks[3] and in particular in Se–templated POMs[1c,1f,1i]. Thus, dimethylamine hydrochloride was used during the combination of $(CH_3)_2Sn^{2+}$ groups with the SeO_3^{2-} anion templates which was employed to restrict the aggregation of more highly symmetrical architectures during the assembly process. Compounds **1** and **2** cannot be isolated by using other cations (e.g., alkali ions).

Finally, different pH value leads to the formation of **1** and **2** thus the impact of the pH should be considered during the one–pot syntheses. From the previously reported studies, the pH value is a known crucial parameter in POT chemistry: a series of available building units toward the formation of the final structures are driven by it and it also provides the chance to obtain Keggin–/Wells−Dawson−type motifs though a pH–dependent synthetic approach[1i,4]. Thus, we analyze the formation of **1** and **2** with the pH value as the single variable: the pH was adjusted from about 5.0 to 3.0 by the dropwise addition of a 2 M HCl solution, and the solution keeps clarification. It changes to turbid when the pH > 5.0 and pH < 3.0. Available Wells−Dawson−type building blocks depend on the pH value: the $\{Se_2W_{12}\}$ and the unique $\{\beta\text{–}Se_2W_{15}\}$ building blocks at pH 3.5 stabilized by $(CH_3)_2Sn^{2+}$ groups for **1**; the $\{\gamma\text{–}Se_2W_{14}\}$ building blocks at pH 4.8 linked by $(CH_3)_2Sn^{2+}$ groups for **2**. In addition, the $(CH_3)_2Sn^{2+}$ groups as linkers with *trans*− and *cis*−$(CH_3)_2Sn^{2+}$ moieties toward to multiple building blocks in solution results the assemblies of dimethyltin–functionalized selenotungstates from nanoclusters to chains.

Some efficient observations during the syntheses of **1**−**2** should be mentioned: (1) The combination of $(CH_3)_2Sn^{2+}$ groups with SeO_3^{2-} heteroanion templates seems to be a potential strategy to build novel dimethyltin–functionalized POTs, which may be due to the inducing effect of the lone pair of electrons in SeO_3^{2-} and the diverse coordinate numbers and geometries of $(CH_3)_2Sn^{2+}$ groups; (2) the correct choice of counteractions which may play an important role in preparation of final architectures; (3) pH–dependent synthetic approach is crucial for the formation of various Dawson-

type building blocks that suitable for the $(CH_3)_2Sn^{2+}$ groups.

References：

[1] (a) J. Yan, J. Gao, D.-L. Long, H. N. Mirasand and L.Cronin, *J. Am. Chem. Soc.*, 2010, **132**, 11410–11411; (b) J. Yan, D.-L. Long and L. Cronin, *Angew. Chem., Int. Ed.*, 2010, **49**, 4117–4120; (c) J. Gao, J. Yan, S. Beeg, D.-L. Long and L. Cronin, *J. Am. Chem. Soc.*, 2012, **135**, 1796–1805; (d) W.-C. Chen, H.-L. Li, X.-L. Wang, K.-Z. Shao, Z.-M. Su and E.-B. Wang, *Chem.–Eur. J.*, 2013, **19**, 11007–11015; (e) J. M. Cameron, J. Gao, L. Vilà-Nadal, D.-L. Long and L. Cronin, *Chem. Commun.*, 2014, 2155–2157; (f) W.-C. Chen, C. Qin, X.-L. Wang, Y.-G. Li, H.-Y. Zang, Y.-Q. Jiao, P. Huang, K.-Z. Shao, Z.-M. Su and E.-B. Wang, *Chem. Commun.*, 2014, 13265–13267; (g) J. M. Cameron, J. Gao, D.-L. Long and L. Cronin, *Inorg. Chem. Front.*, 2014, **1**, 178–185; (h) I. V. Kalinina, E. V. Peresypkina, N. V. Izarova, F. M. Nkala, U. Kortz, N. B. Kompankov, N. K. Moroz and M. N. Sokolov, *Inorg. Chem.*, 2014, **53**, 2076–2082; (i) W.-C. Chen, L.-K. Yan, C.-X. Wu, X.-L. Wang, K.-Z. Shao, Z.-M. Su and E.-B. Wang, *Cryst. Growth Des.*, 2014, **10**, 5099–5110.

[2] (a) F. Hussain, M. Reicke and U. Kortz, *Eur. J. Inorg. Chem.*, 2004, 2733–2738; (b) F. Hussain and U. Kortz, *Chem. Commun.*, 2005, 1191–1193; (c) U. Kortz, F. Hussain and M. Reicke, *Angew. Chem., Int. Ed.,* 2005, **44**, 3773–3777; (d) F. Hussain, U. Kortz, B. Keita, L. Nadjo and M. T. Pope, *Inorg. Chem.*, 2006, **45**, 761–766; (e) S. Reinoso, M. H. Dickman, M. Reicke and U. Kortz, *Inorg. Chem.*, 2006, **45**, 9014–9019; (f) S. Reinoso, M. H. Dickman and U. Kortz, *Inorg. Chem.*, 2006, **45**, 10422–10424; (g) F. Hussain, M. H. Dickman, U. Kortz, B. Keita, L. Nadjo, G. A. Khitrov and A. G. Marshall, *J. Cluster Sci.*, 2007, **18**, 173–191; (h) S. Reinoso, M. H. Dickman, M. F. Matei and U. Kortz, *Inorg. Chem.*, 2007, **46**, 4383–4385; (i) S. Reinoso, M. H. Dickman and U. Kortz, *Eur. J. Inorg. Chem.*, 2009, 947–953; (j) L. F. Piedra-Garza, S. Reinoso, M. H. Dickman, M. M. Sanguineti and U. Kortz, *Dalton Trans.*, 2009, 6231–6234; (k) S. Reinoso, B. S. Bassil, M. Barsukova and U. Kortz, *Eur. J. Inorg. Chem.*, 2010, 2537–2542.

[3] (a) D.-L. Long, P. Kögerler, L. J. Farrugia and L. Cronin, *Angew. Chem. Int. Ed.*, 2003, **42**, 4180–4183; (b) C. Streb, D.-L. Long and L. Cronin, *CrystEngComm*, 2006, **8**, 629–634; (c) D.-L. Long, E. Burkholder and L. Cronin, *Chem. Soc. Rev.*, 2007, **36**, 105–121.

[4] See, for example: (a) C. P. Pradeep, D.-L. Long, C. Streb and L. Cronin, *J. Am. Chem. Soc.*, 2008, **130**, 14946; (b) Y.-Q. Jiao, C. Qin, X.-L. Wang, C.-G. Wang, C.-Y. Sun, H.-N. Wang, K.-Z. Shao and Z.-M. Su, *Chem.–Asian J.*, 2014, **9**, 470−478.

2.3 Crystal Data

Table S2. Crystal Data and Structure Refinements for **1**–**2**.

	1	**2**
Empirical formula	$C_{28}H_{245}N_7Na_{12}O_{268}Se_8Sn_7W_{54}$	$C_{48}H_{390}N_8Na_{10}O_{330}Se_{11}Sn_{16}W_{56}$
M	16635.60	19654.78
λ/Å	0.71073	0.71073
T/K	296(2)	296(2)
Crystal system	Monoclinic	Monoclinic
Space group	$P2_1/c$	$P2_1/n$
a/Å	33.9004(14)	22.382(2)
b/Å	36.2831(14)	20.536(2)
c/Å	28.2841(11)	42.014(4)
α/°	90	90
β/°	110.2392(7)	96.598(2)
γ/°	90	90
V/Å^3	32642(2)	19183(3)
Z	4	2
D_c/Mg m^{-3}	3.385	3.403
μ/mm^{-1}	20.474	18.896
F(000)	29424	17604
θ Range/°	1.39–25.00	1.39–25.00
Measured reflections	189129	108459
Independent reflections	57499	33741
R_{int} after SQUEEZE	0.1269	0.1070
obsd ($I > 2\sigma(I)$)	28323	22276
Goodness-of-fit on F^2	0.986	1.040
$R_1(I > 2\sigma(I))$ [a]	0.0564	0.1000
wR_2 (all data) [b]	0.1277	0.2804

$^{a}R_1 = \sum||F_o| - |F_c||/\sum|F_o|$. $^{b}wR_2 = \{\sum[w(F_o^2 - F_c^2)^2]/\sum[w(F_o^2)^2]\}^{1/2}$.

Single-crystal X-ray diffraction: Single-crystal X-ray diffraction data for **1**–**2** were recorded on a Bruker Apex CCD II area-detector diffractometer with graphite-monochromated $Mo_{K\alpha}$ radiation (λ = 0.71073 Å) at 296(2) K. Absorption corrections were applied using multiscan technique and performed by using the SADABS program[1]. The structures of **1**–**2** were solved by direct methods and refined on F^2 by full-matrix leastsquares methods by using the SHELXTL package[2]. The numbers of lattice water molecules and counter cations for **1**–**2** were estimated by the results of elemental analyses, TG curves, and calculations of electron count in the voids with SQUEEZE[3]. Detailed interpretations for **1**–**2** were shown in CIF files. CCDC 1028650 (**1**) and 1028651 (**2**) contain the supplementary crystallographic data for this paper.

During the refinement for **1**, all the Sn, W, and Se atoms were refined anisotropically, while the rest of the cations and all of the solvent water molecules were just refined isotropically because of their unusual anisotropic thermal parameters and obvious disorder problems. As for all the H atoms in the methyl groups were all directly added to the final molecular formula due to the two tips: 1) the diffraction intensity for all the C atoms is very weak; 2) most C atoms on the tin atoms or $\{C_2H_8N\}$ units exhibit obvious ADP and NPD problems with the anisotropic parameters, they are just refined isotropically. H atoms on lattice water molecules cannot be found from the residual peaks and were directly included in the final molecular formula. The 'omit –3 50' command was used to omit the weak reflections above 50 degree. The highest residual peak, 4.513 eA^3, is near the W53 atom (with the distance of ca. 0.954 eA^3), which is attributed to the series termination errors, but featureless. The deepest hole is –2.517 eA^3.

About 2.5 solvent water molecules, 1 Na^+ cations and 7 $\{C_2H_8N\}^+$ cations were found from the Fourier maps, however, there are still a very large accessible solvent voids in the crystal structure caculated by SQUEEZE subroutine of PLATON software, indicating that some more water molecules and cations should exist in the

structure, but cannot be found from the weak residual electron peaks. Based on the TGA curve, bond valence sum calculations and elemental analyses, another 61.5 water molecules, 11 Na^+ cations and 11 H^+ were included into the molecular formula directly.

```
# SQUEEZE RESULTS (APPEND TO CIF)
loop_
   _platon_squeeze_void_nr
   _platon_squeeze_void_average_x
   _platon_squeeze_void_average_y
   _platon_squeeze_void_average_z
   _platon_squeeze_void_volume
   _platon_squeeze_void_count_electrons
          1      -0.005      -0.004       0.001     12788.0      8084.8
          2       0.219       0.697       0.958        10.5         0.3
          3       0.219       0.803       0.458        10.3        -0.6
          4       0.288       0.080       0.550        11.2        -3.0
          5       0.288       0.420       0.050        11.2        -3.9
          6       0.711       0.580       0.950        11.2        -2.9
          7       0.711       0.920       0.450        11.2        -4.7
          8       0.781       0.197       0.542        10.6        -1.6
          9       0.781       0.303       0.042        10.3        -0.6
_platon_squeeze_details
;
;
```

During the refinement for **2**, all the Sn, W, and Se atoms were refined anisotropically, while the rest of the cations and all of the solvent water molecules were just refined isotropically because of their unusual anisotropic thermal parameters and obvious disorder problems. It was found that the Sn8 can be split into Sn8 and Sn8A with the occupancy 0.8 and 0.2, respectively, thus their thermal parameters (Ueq) should be close to those of other tin centers. As for all the H atoms in the methyl groups were all directly added to the final molecular formula due to the two tips: 1) the diffraction intensity for all the C atoms is very weak; 2) most C atoms on the tin atoms or $\{C_2H_8N\}$ units exhibit obvious ADP and NPD problems with the anisotropic parameters, they are just refined isotropically. H atoms on lattice water molecules cannot be found from the residual peaks and were directly included in the final molecular formula. The 'omit –3 50' command was used to omit the weak

reflections above 50 degree. The highest residual peak, 6.290 eA^3, is near the W12 atom (with the distance of ca. 1.038 eA^3), which is attributed to the series termination errors, but featureless. The deepest hole is –3.298 eA^3.

About 14 solvent water molecules, 2 Na^+ cations and 8 $\{C_2H_8N\}^+$ cations were found from the Fourier maps, however, there are still a very large accessible solvent voids in the crystal structure caculated by SQUEEZE subroutine of PLATON software, indicating that some more water molecules and cations should exist in the structure, but cannot be found from the weak residual electron peaks. Based on the TGA curve, bond valence sum calculations and elemental analyses, another 91 water molecules, 8 Na^+ cations and 8 H^+ were included into the molecular formula directly.

SQUEEZE RESULTS (APPEND TO CIF)
loop_
_platon_squeeze_void_nr
_platon_squeeze_void_average_x
_platon_squeeze_void_average_y
_platon_squeeze_void_average_z
_platon_squeeze_void_volume
_platon_squeeze_void_count_electrons

1	0.500	-0.013	0.000	2494.5	1436.9
2	0.000	0.166	0.500	2494.5	1400.2
3	0.429	0.006	0.461	32.8	23.1
4	0.571	-0.006	0.539	33.1	27.9
5	0.955	0.018	0.697	15.8	13.8
6	0.045	-0.018	0.303	17.2	8.1
7	0.048	0.120	0.727	31.0	9.2
8	0.166	0.080	0.726	5.6	1.4
9	0.648	0.195	0.398	11.4	3.6
10	0.041	0.236	0.289	2.8	2.7
11	0.541	0.264	0.789	3.3	2.5
12	0.148	0.305	0.898	11.4	1.5
13	0.547	0.381	0.226	31.4	8.4
14	0.666	0.420	0.226	5.8	0.9
15	0.929	0.494	0.961	32.8	32.1
16	0.453	0.486	0.196	15.4	7.8
17	0.071	0.506	0.039	33.1	13.0
18	0.545	0.518	0.803	16.5	9.1
19	0.452	0.620	0.773	30.6	17.2
20	0.333	0.580	0.774	4.9	0.2
21	0.852	0.695	0.102	11.4	3.3

```
        22      0.459     0.736     0.211      2.8       5.0
        23      0.959     0.764     0.711      3.2       5.2
        24      0.352     0.805     0.602     11.4       1.9
        25      0.952     0.879     0.273     29.9      14.1
        26      0.833     0.920     0.274      5.1       0.2
_platon_squeeze_details
;
;
```

References：

[1] Sheldrick, G. *SADABS*; ver. 2.10; University of Gottingen: Göttingen, Germany, **2003**.

[2] Sheldrick, G. M. *SHELXL-97, Program for the Refinement of Crystal Structure*; University of Gottingen: Göttingen, Germany, **1993**.

[3] Spek, A. L. *PLATON, A Multipurpose Crystallographic Tool*; Utrecht University, Utrecht, The Netherlands, **2003**.

2.4 Structures of 1-2

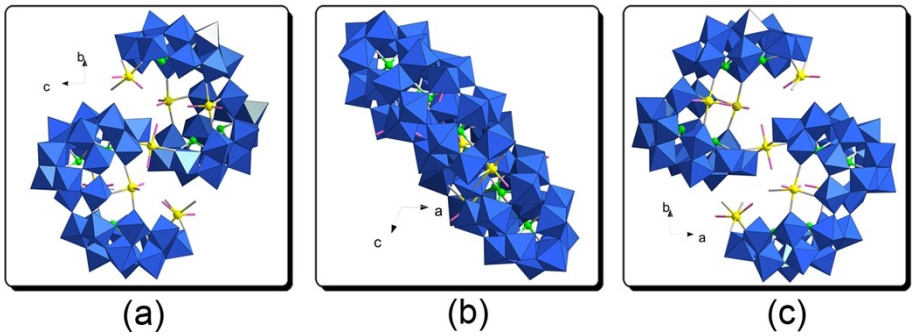

Fig. S1. Structure of **1a** in different orientations: (a) bc-view, (b) ac-view, (c) ab-view.

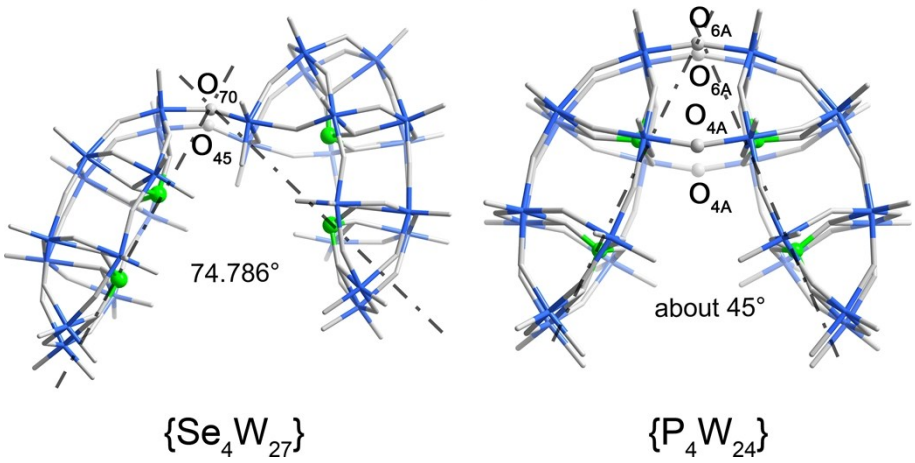

Fig. S2. The comparison of dimeric fragments: the $\{Se_4W_{27}\}$ fragment in **1a** and $\{P_4W_{24}\}$ fragment.

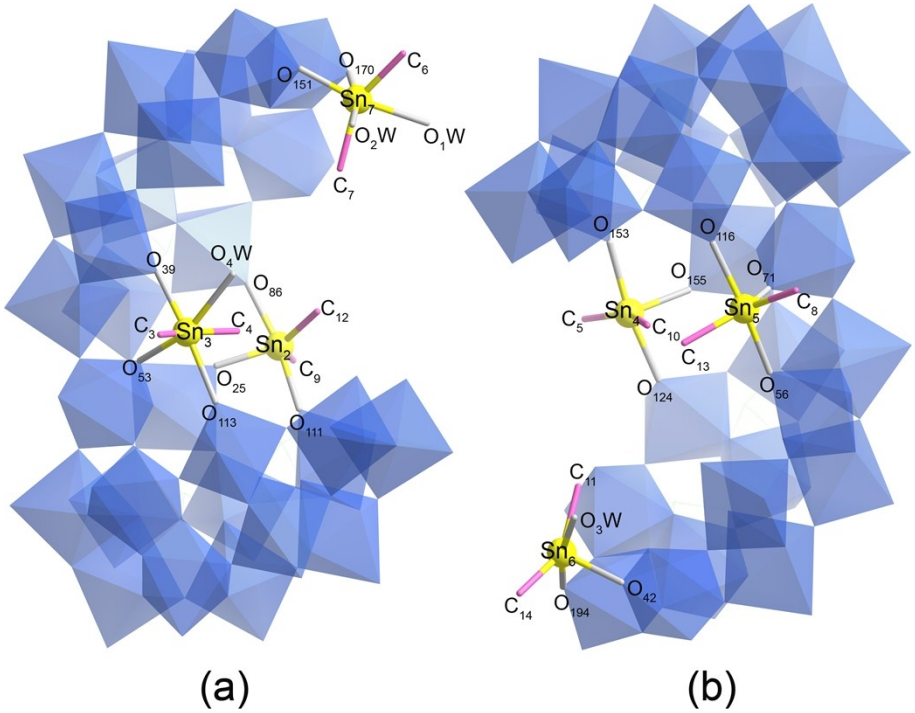

Fig. S3. Structure of two types of dimethyltin−containing $\{Sn_3Se_4W_{27}\}$ units in **1a**.

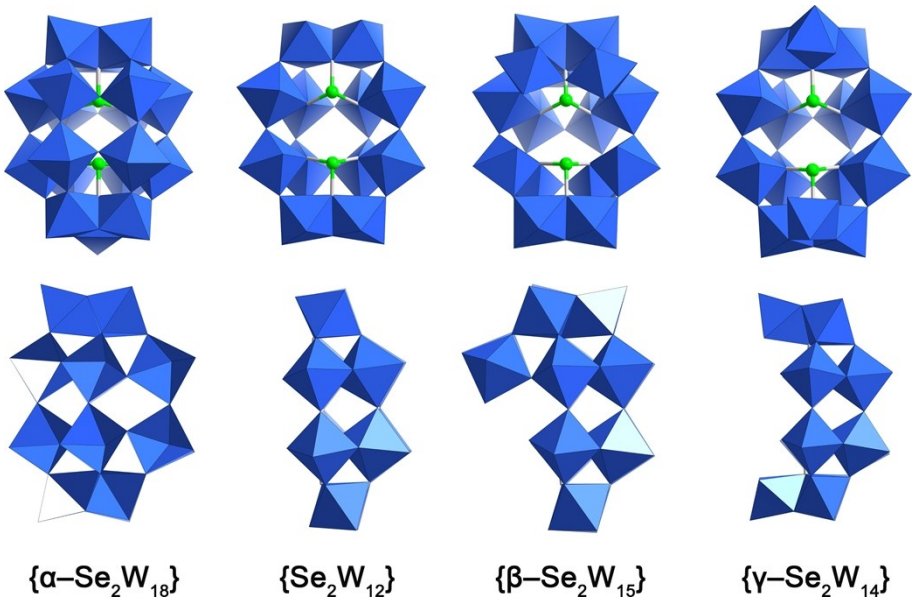

Fig. S4. The comparison of Se−templated Wells−Dawson−type polyoxotungstate building blocks. Top: front-view, bottom: side-view.

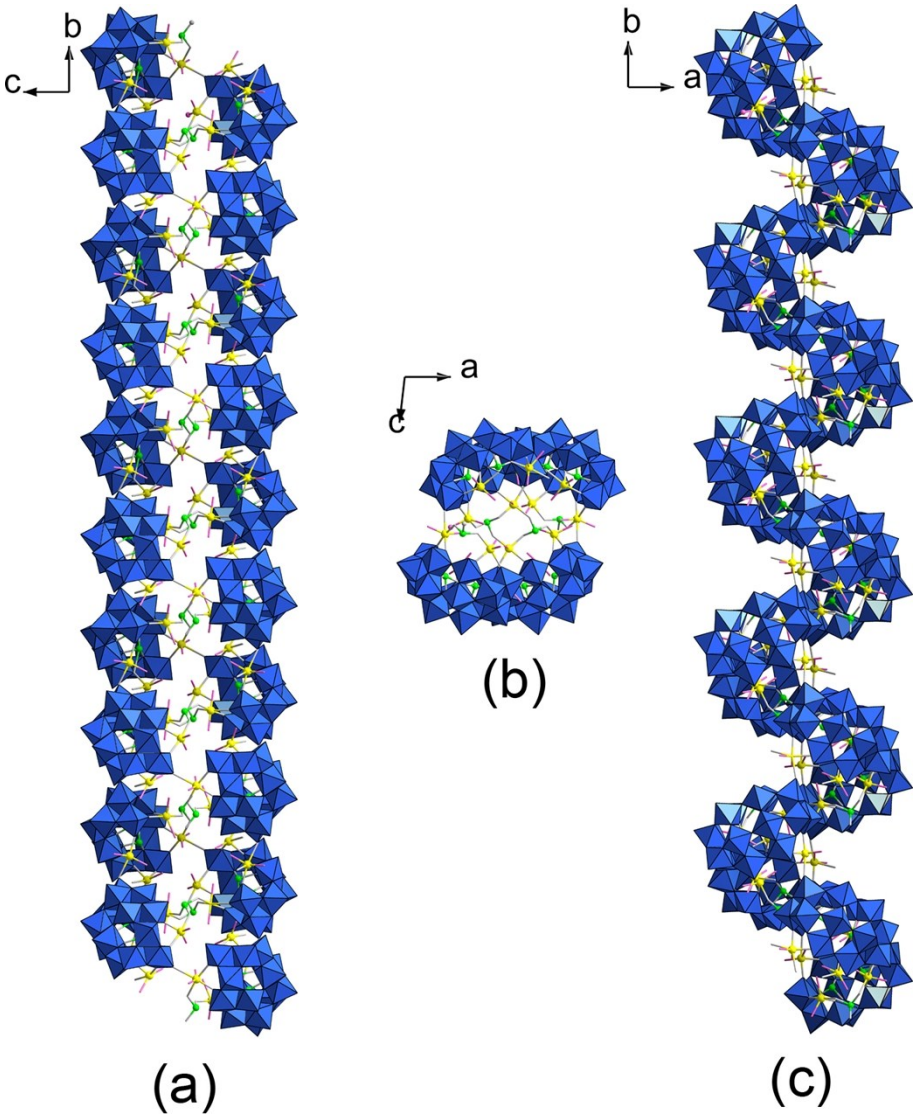

Fig. S5. Structure of **2** in different orientations: (a) *bc*-view, (b) *ac*-view, (c) *ab*-view

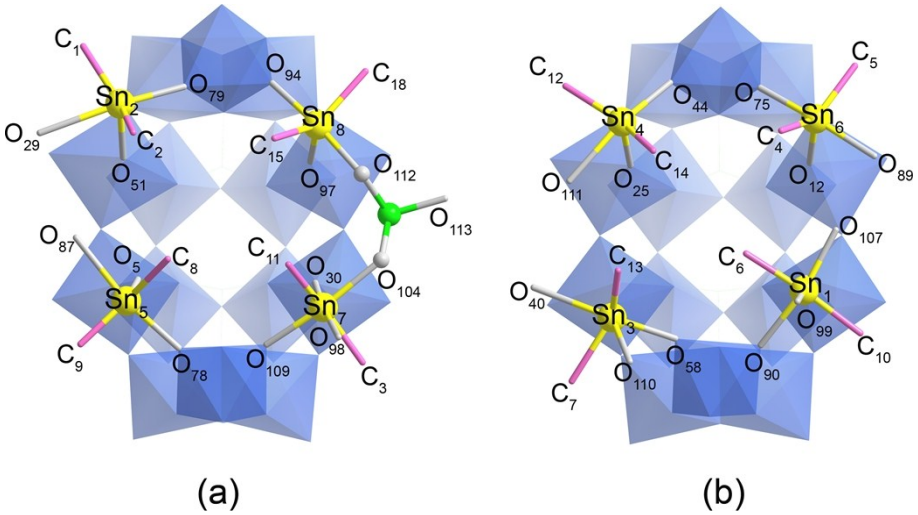

Fig. S6. Structure of two types of dimethyltin−containing Wells−Dawson−type units in **2a**. (a) **Type A**, (b) **Type B**.

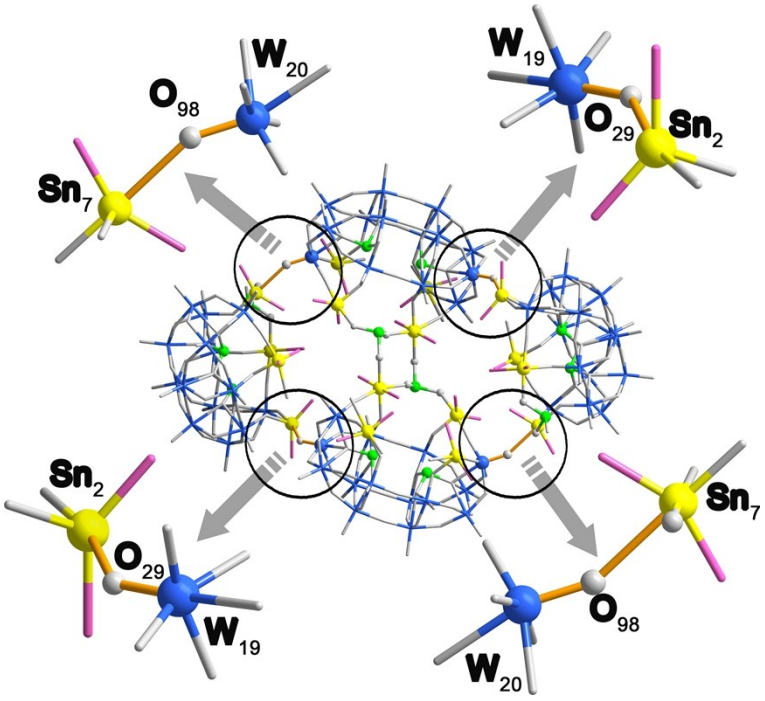

Fig. S7. Connection patterns between two types of dimethyltin−containing Wells−Dawson−type units (**Type A** and **Type B)** in **2a**.

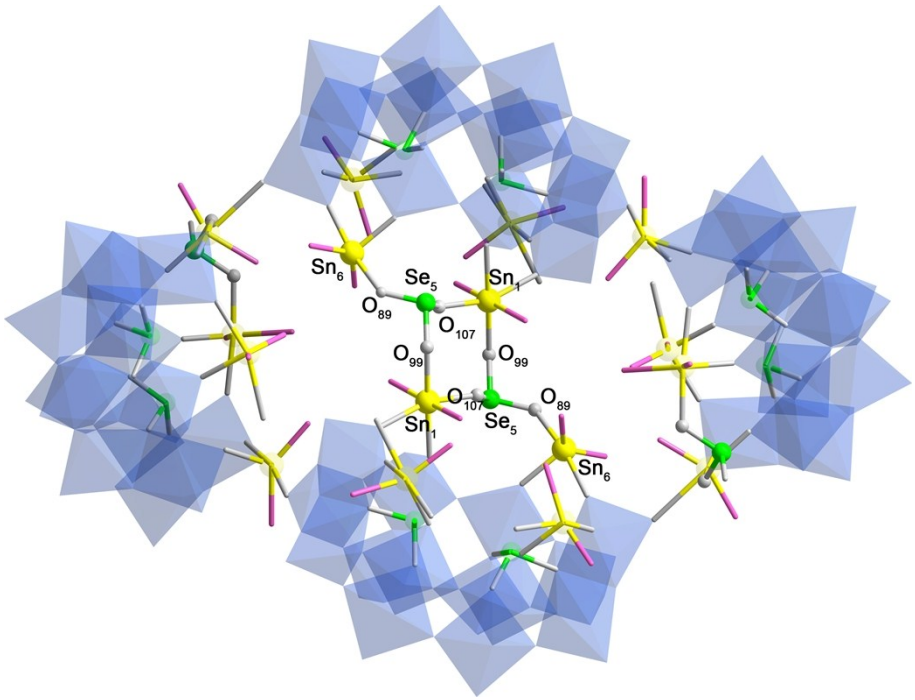

Fig. S8. Connection patterns between two **Type B** in **2a**.

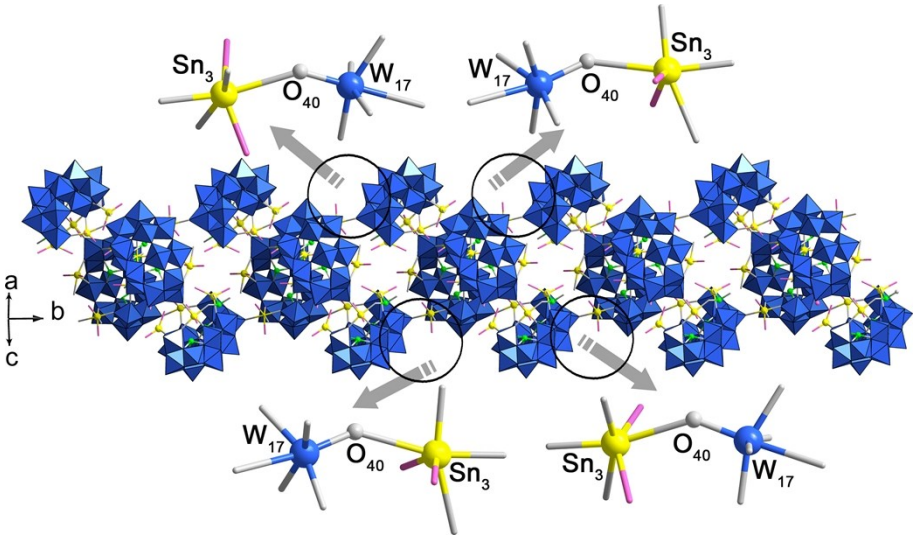

Fig. S9. Connection patterns of chain of **2**.

2.5 The BVS Calculation Result of All the Oxygen and Selenium Atoms

Table S3. The BVS calculation results of all the oxygen atoms in **1**.

Oxygen Code	Bond Valence	Protonation Degree	Oxygen Code	Bond Valence	Protonation Degree
O_{99}	1.372	1	O_{180}	1.354	1
O_{139}	1.402	1	O_{188}	1.417	1
O_{154}	1.321	1	O_{191}	0.464	2
O_{169}	1.265	1	O_{200}	1.346	1
O_{172}	0.477	2			
Total 11 protons per cluster					

Table S4. The BVS calculation results of all the oxygen atoms in **2**.

Oxygen Code	Bond Valence	Protonation Degree	Oxygen Code	Bond Valence	Protonation Degree
O_{31}	1.317	1	O_{81}	1.346	1
O_{40}	1.325	1	O_{101}	1.282	1
Total 8 protons per cluster					

Table S5. The BVS calculation result of all Se^{IV} atoms in **1** and **2**.

Compound **1**			
Code	Bond Valence	Code	Bond Valence
Se_1	4.002	Se_2	3.957
Se_3	3.812	Se_4	4.318
Se_5	3.616		
Compound **2**			
Code	Bond Valence	Code	Bond Valence
Se_1	3.940	Se_2	4.079
Se_3	4.019	Se_4	3.973
Se_5	3.787	Se_6	4.025
Se_7	3.758	Se_8	3.964

2.6 Selected Bond Lengths and Angles for the Tin Atoms in 1-2.

Table S6. Selected bond lengths [Å] and angles [°] for the tin atoms in **1**–**2**.

1		**2**	
Sn(1)-C(1)	2.12(3)	Sn(1)-O(107)#1	2.06(3)
Sn(1)-C(2)	2.12(3)	Sn(1)-C(10)	2.14(4)
Sn(1)-O(22)	2.196(14)	Sn(1)-C(6)	2.17(7)
Sn(1)-O(58)	2.227(16)	Sn(1)-O(90)	2.21(3)
Sn(1)-O(81)	2.247(16)	Sn(1)-O(22)	2.22(3)
Sn(1)-O(127)	2.291(15)	Sn(1)-O(99)	2.30(3)
C(1)-Sn(1)-C(2)	***176.7(12)***	***C(10)-Sn(1)-C(6)***	***175(2)***
Sn(2)-O(25)	2.038(15)	Sn(2)-C(1)	2.04(4)
Sn(2)-C(9)	2.07(3)	Sn(2)-O(51)	2.08(2)
Sn(2)-C(12)	2.13(3)	Sn(2)-O(79)	2.10(3)
Sn(2)-O(86)	2.163(15)	Sn(2)-C(2)	2.10(6)
Sn(2)-O(111)	2.191(14)	***C(1)-Sn(2)-C(2)***	***143.8(19)***
C(9)-Sn(2)-C(12)	***133.2(10)***	Sn(3)-O(58)	2.05(3)
Sn(3)-O(113)	2.025(17)	Sn(3)-O(36)	2.05(2)
Sn(3)-C(3)	2.06(3)	Sn(3)-C(13)	2.08(6)
Sn(3)-C(4)	2.10(3)	Sn(3)-C(7)	2.32(6)
Sn(3)-O(39)	2.118(14)	Sn(3)-O(17W)	2.405(10)
Sn(3)-O(53)	2.334(15)	***C(13)-Sn(3)-C(7)***	***136(2)***
Sn(3)-O(4W)	2.554(17)	Sn(4)-O(25)	2.04(2)
C(3)-Sn(3)-C(4)	***157.4(13)***	Sn(4)-O(44)	2.05(3)
Sn(4)-O(155)	1.993(19)	Sn(4)-C(14)	2.09(8)
Sn(4)-C(5)	2.16(4)	Sn(4)-C(12)	2.17(9)
Sn(4)-O(124)	2.198(15)	Sn(4)-O(18W)	2.410(10)
Sn(4)-O(153)	2.241(16)	***C(14)-Sn(4)-C(12)***	***145(3)***
Sn(4)-C(10)	2.28(4)	Sn(5)-C(9)	1.94(7)
C(5)-Sn(4)-C(10)	***154.7(15)***	Sn(5)-O(5)	2.02(2)
Sn(5)-O(71)	2.013(15)	Sn(5)-O(78)	2.09(3)

Sn(5)-O(56)	2.153(14)	Sn(5)-C(8)	2.21(7)
Sn(5)-C(13)	2.15(4)	Sn(5)-O(16W)	2.46(3)
Sn(5)-C(8)	2.17(3)	***C(9)-Sn(5)-C(8)***	***140(3)***
Sn(5)-O(116)	2.227(14)	Sn(6)-O(12)	2.00(2)
C(13)-Sn(5)-C(8)	***123.7(12)***	Sn(6)-C(4)	2.08(6)
Sn(6)-C(14)	2.04(4)	Sn(6)-C(5)	2.18(5)
Sn(6)-O(42)	2.044(14)	Sn(6)-O(75)	2.18(3)
Sn(6)-O(194)	2.067(18)	Sn(6)-O(89)	2.20(3)
Sn(6)-C(11)	2.10(3)	***C(4)-Sn(6)-C(5)***	***139(2)***
C(14)-Sn(6)-C(11)	***145.6(12)***	Sn(7)-C(11)	2.01(5)
Sn(7)-O(170)	2.081(17)	Sn(7)-O(30)	2.06(3)
Sn(7)-C(7)	2.06(3)	Sn(7)-C(3)	2.08(5)
Sn(7)-O(151)	2.074(16)	Sn(7)-O(109)	2.09(4)
Sn(7)-C(6)	2.21(4)	Sn(7)-O(104)	2.26(3)
C(7)-Sn(7)-C(6)	***141.7(14)***	***C(11)-Sn(7)-C(3)***	***151(2)***
		Sn(8)-O(97)	2.03(3)
		Sn(8)-O(94)	2.10(3)
		Sn(8)-O(112)	2.20(3)
		Sn(8)-C(18)	2.199(10)
		Sn(8)-C(15)	2.498(10)
		C(18)-Sn(8)-C(15)	***127(2)***

Section 3 Experimental Section

3.1 Materials and Physical Measurements

Characterization: Elemental analysis of Na, Sn, Se, and W were performed with a Leaman inductively coupled plasma (ICP) spectrometer; C and N were performed on a Perkin-Elmer 2400 CHN elemental analyzer. IR spectra were recorded on an Alpha Centauri FTIR spectrophotometer on pressed KBr pellets in the range 400~4000 cm^{-1}. Water contents were determined by TG analyses on a PerkinElmer TGA7 instrument in flowing N_2 with a heating rate of 10 °C min^{-1}. Electrospray ionization mass spectrometry was carried out on a Bruker Micro TOF-QII instrument (1 mg/mL).

Electrochemical experiments: Electrochemical measurements were carried out on a CHI 660 electrochemical workstation at room temperature. Thrice-distilled water was used throughout the experiments. All solutions were deaerated by bubbling pure argon prior to the experiments and the electrochemical cell was kept under an argon atmosphere throughout the experiment. A conventional three-electrode system was used with a 1.5 mm glassy carbon working electrode, an Ag/AgCl used as electrode, and a platinum wire counterelectrode. The glassy carbon working electrodes were polished with alumina on polishing pads, rinsed with distilled water, and sonicated in H_2O before each experiment. The scan rate was 20~500 mV s^{-1}. All potentials were measured and reported versus Ag/AgCl. Solutions **1** in 0.5 M H_2SO_4/Na_2SO_4 (pH = 2.50, 3.50 and 4.50) were used. A pHS-25B pH meter was used for pH measurements.

Photocatalytic Measurements: Photocatalytic reactions were carried out in a Pyrex inner-irradiation-type reaction vessel with a magnetic stirrer at room temperature. The reactant solution was evacuated using N_2 several times to ensure complete air removal and then irradiated by using a 500 W mercury lamp. The produced H_2 was analyzed by a GC9800 instrument with a thermal conductivity detector and a 5 Å molecular sieve column (2 mm × 2 mm) using N_2 as carrier gas.

3.2 UV-Vis spectra

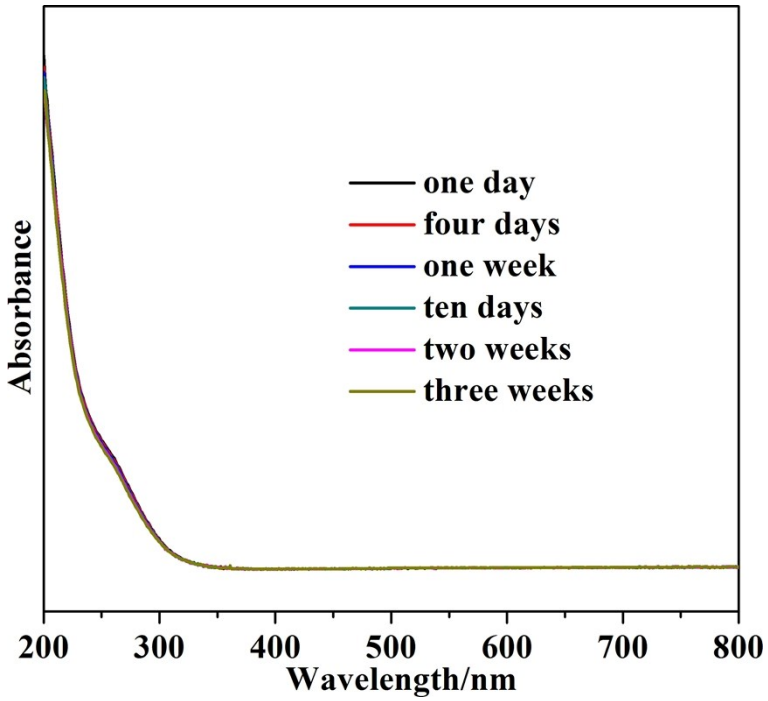

Fig. S10. UV-Vis spectra of kept at room temperature for three weeks.

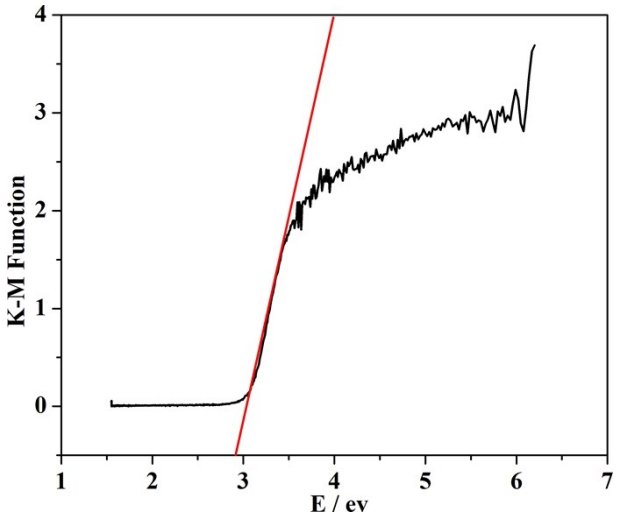

Fig. S11. The diffuse reflectance UV-vis-NIR spectra of K-M function *vs.* energy (eV) of **1**.

3.3 ESI-MS

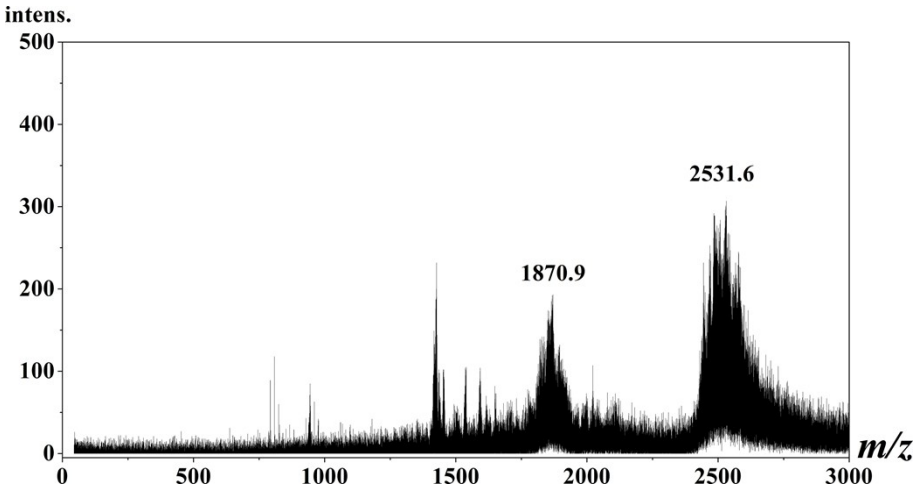

Fig. S12. ESI-MS of **1** in H_2O.

Table S7. Assignment of peaks in negative mode Mass spectrum of **1**.

Observed m/z	Calculated m/z	Charge	Molecular mass	Polyanion
1870.9	1870.2	−8	14961.5	$\{(C_2H_8N)NaH_9[\{Sn(CH_3)_2\}_4\{Sn(CH_3)_2(H_2O)\}_2\{Sn(CH_3)_2(H_2O)_2\}Se_8W_{54}O_{191}(OH)_7(H_2O)_2]\}^{8-}$
2531.6	2531.8	−6	15190.5	$\{(C_2H_8N)_3Na_4H_5[\{Sn(CH_3)_2\}_4\{Sn(CH_3)_2(H_2O)\}_2\{Sn(CH_3)_2(H_2O)_2\}Se_8W_{54}O_{191}(OH)_7(H_2O)_2(H_2O)_4]\}^{6-}$

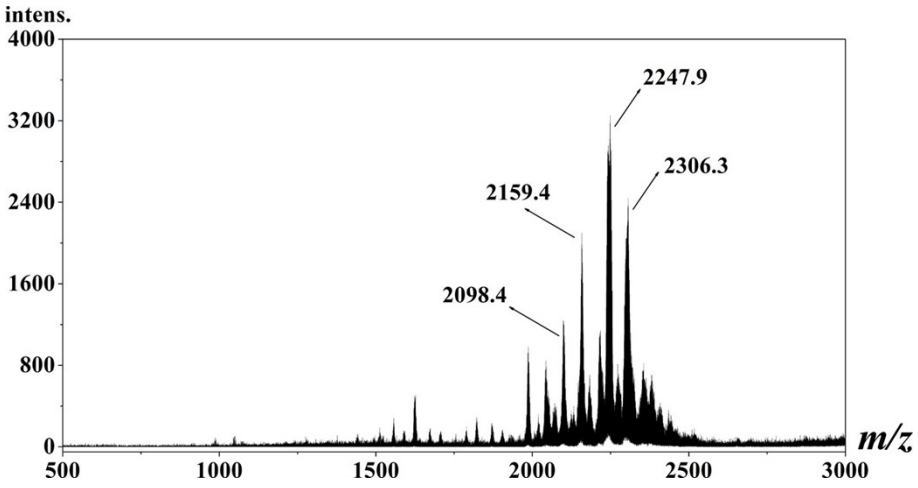

Fig. S13. ESI-MS of **2** in H_2O.

Table S8. Assignment of peaks in negative mode Mass spectrum of **2**.

Observed *m*/*z*	Calculated *m*/*z*	Charge	Molecular mass	Polyanion
2098.4	2098.4	−2	4196.8	$\{[\{Sn(CH_3)_2(H_2O)\}_2\{Sn(CH_3)_2\}_2Se_2W_{14}O_{50}(OH)_2]\}^{2-}$
2159.4	2159.7	−2	4319.3	$\{NaH_2[\{Sn(CH_3)_2(H_2O)\}\{Sn(CH_3)_2\}_3Se_{2.5}W_{14}O_{52.5}(OH)_2(H_2O)_2]\}^{2-}$
2247.9	2247.2	−2	4494.3	$\{(C_2H_8N)Na_2[\{Sn(CH_3)_2(H_2O)\}\{Sn(CH_3)_2\}_3Se_{2.5}W_{14}O_{52.5}(OH)_2(H_2O)_8\}^{2-}$
	2247.9	−2	4495.8	$\{Na_2[\{Sn(CH_3)_2(H_2O)\}_2\{Sn(CH_3)_2\}_2Se_3W_{14}O_{53}(OH)_2(H_2O)_7]\}^{2-}$
2306.3	2306.2	−2	4612.3	$\{(C_2H_8N)_3\{Sn(CH_3)_2(H_2O)\}\{Sn(CH_3)_2\}_3Se_{2.5}W_{14}O_{52.5}(OH)_2](H_2O)_{12}\}^{2-}$
	2306.9	−2	4613.8	$\{H_2[\{Sn(CH_3)_2(H_2O)\}_2\{Sn(CH_3)_2\}_2Se_3W_{14}O_{53}(OH)_2(H_2O)_{16}]\}^{2-}$

3.4 Cyclic Voltammetry

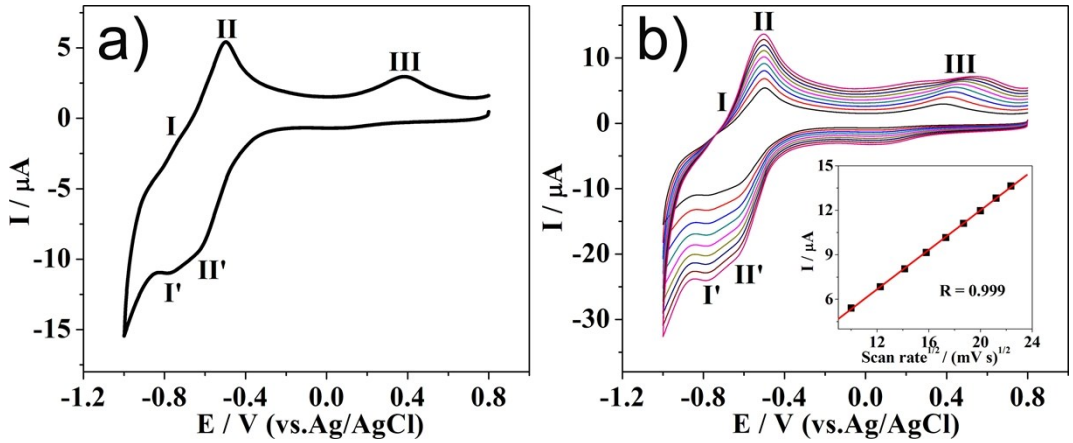

Fig. S14. Cyclic voltammograms of **1** in aqueous 0.5 M H_2SO_4/Na_2SO_4 solutions (pH = 4.50). POM concentrations = 5×10^{-4} M. The scan rate was 100 mV s^{-1} (a). Cyclic voltammograms of **1** at different scan rates (b): from inside to out: 100, 150, 200, 250, 300, 350, 400, 450 and 500 mV s^{-1}. Inset: representation of the current as a function of the square root of the scan rate. The linear relationship indicates that the processes are diffusion controlled. The working electrode was glassy carbon, and the reference electrode was Ag/AgCl.

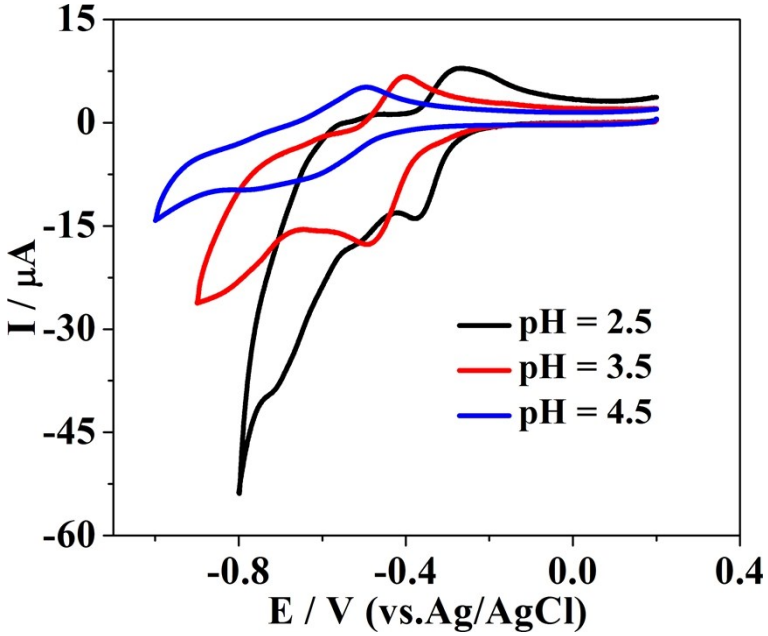

Fig. S15. Cyclic voltammograms of **1** at different pH values: pH 2.5 (black), pH 3.5 (red), pH 4.5 (blue) in 0.5 M H_2SO_4/Na_2SO_4 solution. POM concentrations = 5×10^{-4}

M. The scan rate was 100 mV s^{-1}. The working electrode was glassy carbon, and the reference electrode was Ag/AgCl.

Table S9. Redox Peak Potentials for the First Tungsten Waves Determined by Cyclic Voltammetry in 0.5 M H_2SO_4/Na_2SO_4 solution at pH 2.50, 3.50, and 4.50 for **1**.

pH	E_{pa} (V)	E_{pc} (V)	$E_{1/2}$ (V)	ΔE_p (mV)
2.5	−0.283	−0.378	−0.331	95
3.5	−0.403	−0.489	−0.446	86
4.5	−0.499	−0.609	−0.554	110

Table S10. Reduction Peak Potentials, E_{pc}, for all the Tungsten Waves Determined by Cyclic Voltammetry at pH 2.50, 3.50, and 4.50 for **1**.

pH	E_{pc1} (V)	E_{pc2} (V)	E_{pc3} (V)
2.5	−0.378	−0.507	−0.712
3.5	−0.489	−0.622	
4.5	−0.609	−0.784	

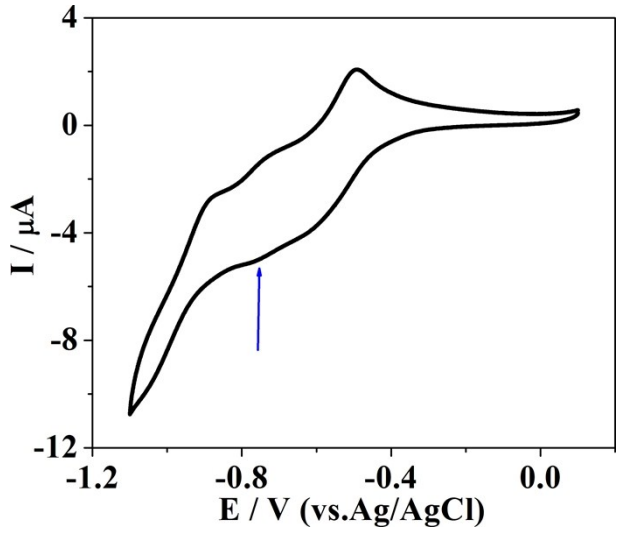

Fig. S16. Cyclic voltammograms of **1** at pH 4.50 in 0.5 M H_2SO_4/Na_2SO_4 solution. POM concentrations = 5×10^{-4} M. The scan rate was 20 mV s^{-1}. The working electrode was glassy carbon, and the reference electrode was Ag/AgCl.

Electrochemistry: Cyclic voltammetry (CV) experiments were performed to examine the redox properties of **1** in 0.5 M H_2SO_4/Na_2SO_4 solutions pH = 4.50. The waves associated with the redox processes of W^{VI} centers between –0.784 and –0.499 V as well as the oxidation of Se^{IV} centers at +0.387 (*vs* Ag/AgCl), which are in good agreement with reported selenotungstate compounds.[1] In a sulfate pH 4.50 medium, the CV of **1** (5×10^{-4} M) (Fig. S14) at a scan rate of 100 mV s^{-1} shows the main characteristic peaks associated with W centered redox couples in the region –1.000 to +0.800 V of potential values *vs* Ag/AgCl. Two separated redox couples of waves at $E_{1/2}$ = –0.756 V (I/I') and $E_{1/2}$ = –0.554 V (II/II') [$E_{1/2} = (E_{pa} + E_{pc})/2$], corresponding to the redox processes of W^{VI} centers, respectively (Table S9). It is well-known for the electrochemical behavior of the majority of the POMs that the number and the characteristics of these W waves depend on the pH[2]. As expected, the CV pattern of W–waves moves toward negative potentials when the pH ranges from 2.50 to 4.50 (Fig. S15). In addition, the redox peak potentials for the first tungsten waves (II/II') gradually clear with a larger current intensity when the pH is sequentially decreased from 4.50 to 2.50 (Fig. S15 and Table S9). Some other Dawson–type selenotungstate clusters, such as $\{Se_4W_{36}\}$[1e], which also show one tungsten wave possesses unforgettable and sharp redox peak potential compared to the others. Furthermore, Table S10 contains the CV characteristics of reduction peak potential differences for all the tungsten waves as a function of pH. Considering just the reduction scan, the second and third W−waves gradually merge when the pH is sequentially increased from 2.5 to 4.5. Interestingly, still one "merged" single reduction wave (Fig. S16) could be observed at pH 4.50 at a slow scan rate of 20 mV s^{-1}. This observation is remarkable because usually W−waves are more likely to split rather than merge upon increasing the electrolyte pH. The same behavior as a function of pH has been previously reported, namely, for the large, macrocyclic $[H_7P_8W_{48}O_{184}]^{33-}$[3a], Ni_{14}–containing POTs $[Ni_{14}(OH)_6(H_2O)_{10}(HPO_4)_4(P_2W_{15}O_{56})_4]^{34-}$[3b], etc.. In the positive branch of the CV of **1**, it can be observed an oxidation peak located at +0.387 V (III) *vs* Ag/AgCl, which can be assigned to the oxidation of the Se^{IV} centres[1]. As a matter of fact, no feature was observed in CV which could be associated with

reduction of the Sn centers as previously reported in dimethyltin−containing POMs[4] by Kortz et al.. After increasing the scan rates, from 100 to 500 mV s^{-1} (Fig. S14b), the peak currents were proportional to the square root of the scan rate, demonstrating that the redox process becomes diffusion-controlled (Fig. S14b), similar behaviors were observed in the case of the other compounds[2].

References:

[1] (a) J. Gao, J. Yan, S. Beeg, D.-L. Long and L. Cronin, *J. Am. Chem. Soc.*, 2012, **135**, 1796–1805; (b) W.-C. Chen, H.-L. Li, X.-L. Wang, K.-Z. Shao, Z.-M. Su and E.-B. Wang, *Chem.–Eur. J.*, 2013, **19**, 11007–11015; (c) W.-C. Chen, C. Qin, X.-L. Wang, Y.-G. Li, H.-Y. Zang, Y.-Q. Jiao, P. Huang, K.-Z. Shao, Z.-M. Su and E.-B. Wang, *Chem. Commun.*, 2014, 13265–13267; (d) J. M. Cameron, J. Gao, D.-L. Long and L. Cronin, *Inorg. Chem. Front.*, 2014, **1**, 178–185; (e) W.-C. Chen, L.-K. Yan, C.-X. Wu, X.-L. Wang, K.-Z. Shao, Z.-M. Su and E.-B. Wang, *Cryst. Growth Des.*, 2014, **10**, 5099–5110.

[2] (a) D. Jabbour, B. Keita, I. M. Mbomekalle, L. Nadjo and U. Kortz, *Eur. J. Inorg. Chem.,* 2004, 2036; (b) L.-H. Bi, E.-B. Wang, J. Peng, R.-D. Huang, L. Xu and C.-W. Hu, *Inorg. Chem.,* 2000, **39**, 671; (c) B. S. Bassil, U. Kortz, A. S. Tigan, J. M. ClementeJuan, B. Keita, P. Oliveira and L. Nadjo, *Inorg. Chem.,* 2005, **44**, 9360; (d) I. M. Mbomekalle, B. Keita, M. Nierlich, U. Kortz, P. Berthet and L. Nadjo, *Inorg. Chem.,* 2003, **42**, 5143; (e) B. Keita, Y.-W. Lu, L. Nadjo and R. Contant, *Electrochem. Commun.,* 2000, **2**, 720.

[3] (a) B. Keita, Y. W. Lu, L. Nadjo and R. Contant, *Electrochem. Commun.,* 2000, **2**, 720; (b) M. Ibrahim, Y. Xiang, B. S. Bassil, Y. Lan, A. K. Powell, P. de Oliveira, B. Keita and U. Kortz, *Inorg. Chem.,* 2013, **52**, 8399.

[4] F. Hussain, U. Kortz, B. Keita, L. Nadjo and M. T. Pope, *Inorg. Chem.*, 2006, **45**, 761–766.

3.5 Photocatalytic Hydrogen Evolution

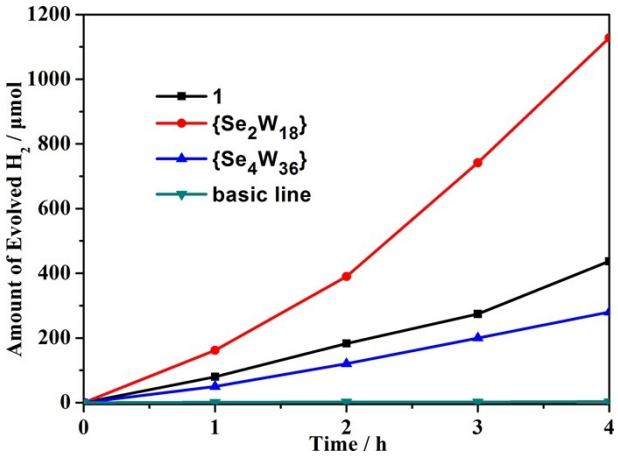

Fig. S17. Dependence of H_2 production on irradiation time with the use of **1** (black), $\{Se_2W_{18}\}$ (red), and $\{Se_4W_{36}\}$ (blue) as photocatalysts (100 mg). The experiments were performed under 500 W mercury lamp irradiation in methanol (30 mL) in 150 mL of water (5/1, v/v).

The H_2 evolution rate with the use of **1** over 4 h (TON 72) is higher than that of the isolated Wells–Dawson–type selenotungstate clusters, $\{Se_2W_{18}\}$ or $\{Se_4W_{36}\}$ (The corresponding TON over 4 h under the same conditions were 56 or 27, respectively). It is should mentioned that the monomer $\{Se_2W_{18}\}$ exhibits higer effects on the H_2 evolution than that of dimer $\{Se_4W_{36}\}$ maily due to the following reasons: in monomer $\{Se_2W_{18}\}$, each of the four tungsten units at the equatorial position has two terminal ligands, and these extra terminal ligand positions are occupied by water or oxo ligands (*Cryst. Growth Des.*, 2014, **10**, 5099–5110) while in dimer $\{Se_4W_{36}\}$, all the oxygen atoms remain no protonation (*Cryst. Growth Des.*, 2014, **10**, 5099–5110). The H_2O molecules bonded directly to W in monomer $\{Se_2W_{18}\}$ that improves transportation of charge carriers and the subsequent reduction of proton to H^+/H_2. This phenomenon has already found in other works: (a) *J. Am. Chem. Soc.*, 2011, **133**, 6934−6937; (b) *Chem. Commun.*, 2012, **48**, 5733−5735; (c) *Angew. Chem., Int. Ed.*, 2011, **50**, 7238−7266; (d) *J. Am. Chem. Soc.*, 1979, **101**, 2027−2038.

Section 4 Supplementary Physical Characterizations

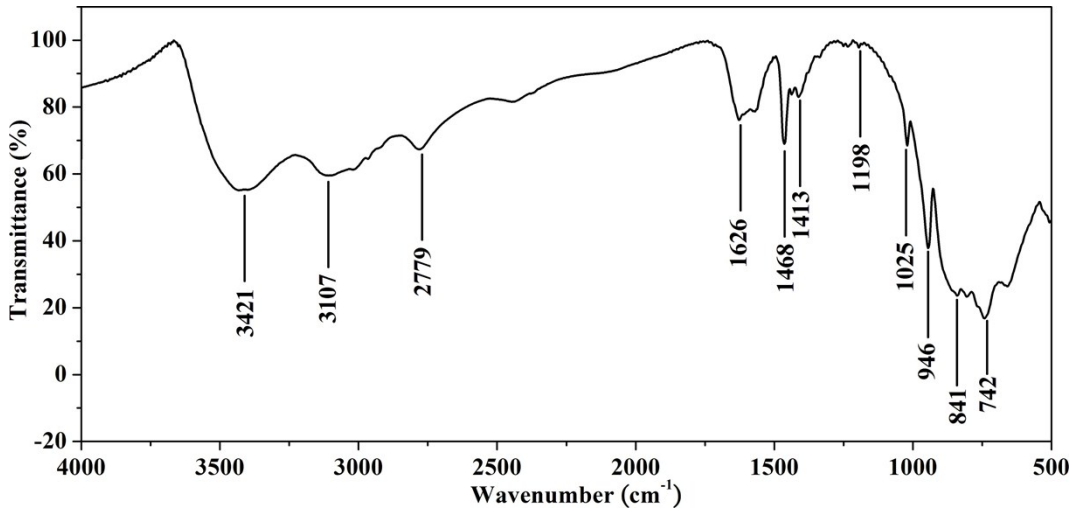

Fig. S18. IR spectrum of **1**: The characteristic peaks at 1025, 946, 841, and 742 cm^{-1} are ascribed to vibrations of ν(Se–O), ν(W=Od), ν(W–Ob), and ν(W–Oc), respectively. The broad peak at 3421 cm^{-1} and the strong peak at 1626 cm^{-1} are attributed to the lattice water molecules and aqua ligands. The peaks at 3107, 2779, 1468, and 1413 cm^{-1} are assigned to $\{C_2H_8N\}$ organic molecules. The single peak of weak intensity around 1198 cm^{-1}, which is characteristic of methyltin(IV) derivatives and can be assigned to the symmetrical bending vibration of the methyl groups according to the previously reported dimethyltin-functionalized POM species.

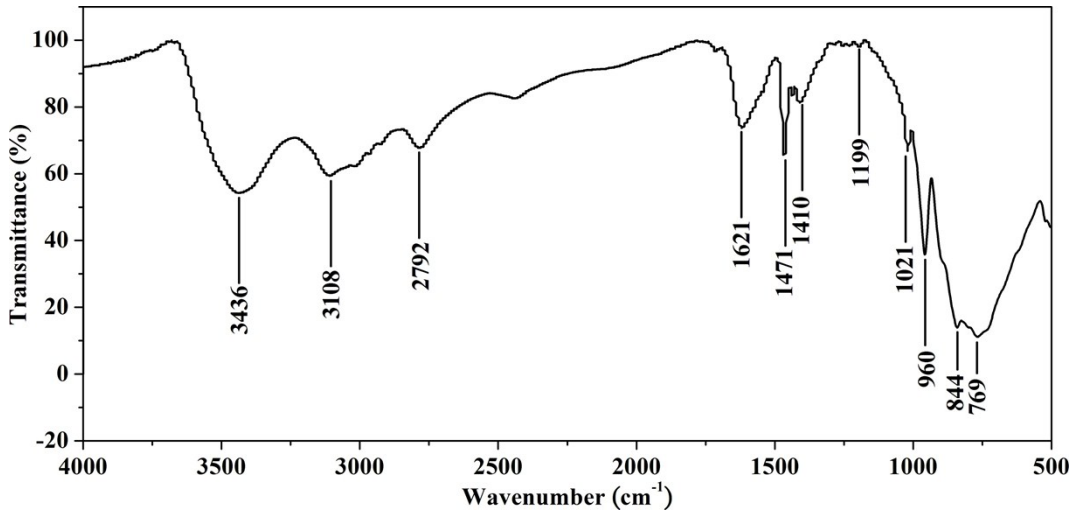

Fig. S19. IR spectrum of **2**: The characteristic peaks at 1021, 960, 844, and 769 cm^{-1} are ascribed to vibrations of ν(Se–O), ν(W=Od), ν(W–Ob), and ν(W–Oc),

respectively. The broad peak at 3436 cm^{-1} and the strong peak at 1621 cm^{-1} are attributed to the lattice water molecules and aqua ligands. The peaks at 3108, 2792, 1471, and 1410 cm^{-1} are assigned to $\{C_2H_8N\}$ organic molecules. The single peak of weak intensity around 1199 cm^{-1}, which is characteristic of methyltin(IV) derivatives and can be assigned to the symmetrical bending vibration of the methyl groups according to the previously reported dimethyltin-functionalized POM species.

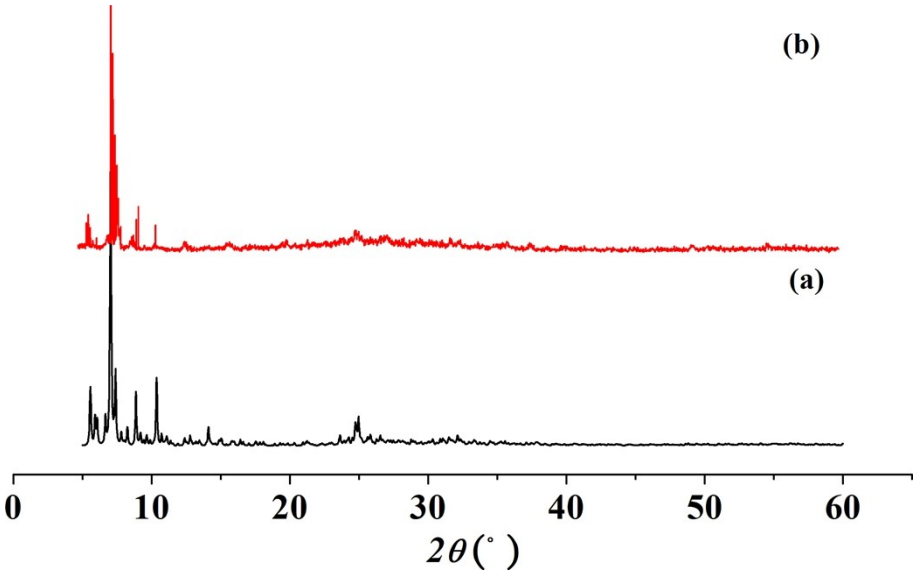

Fig. S20. The XRPD patterns for simulated (a) and as-synthesized (b) of **1**.

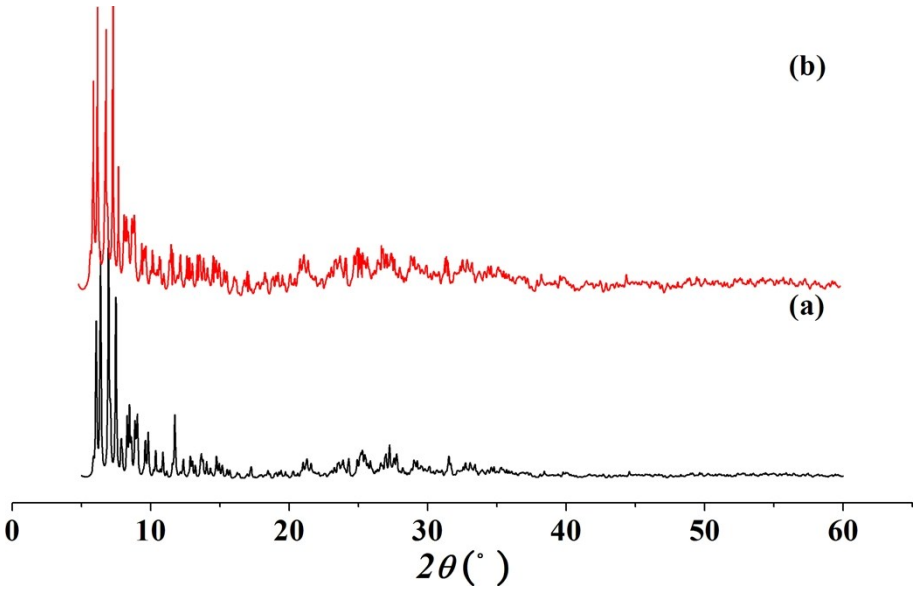

Fig. S21. The XRPD patterns for simulated (a) and as-synthesized (b) of **2**.

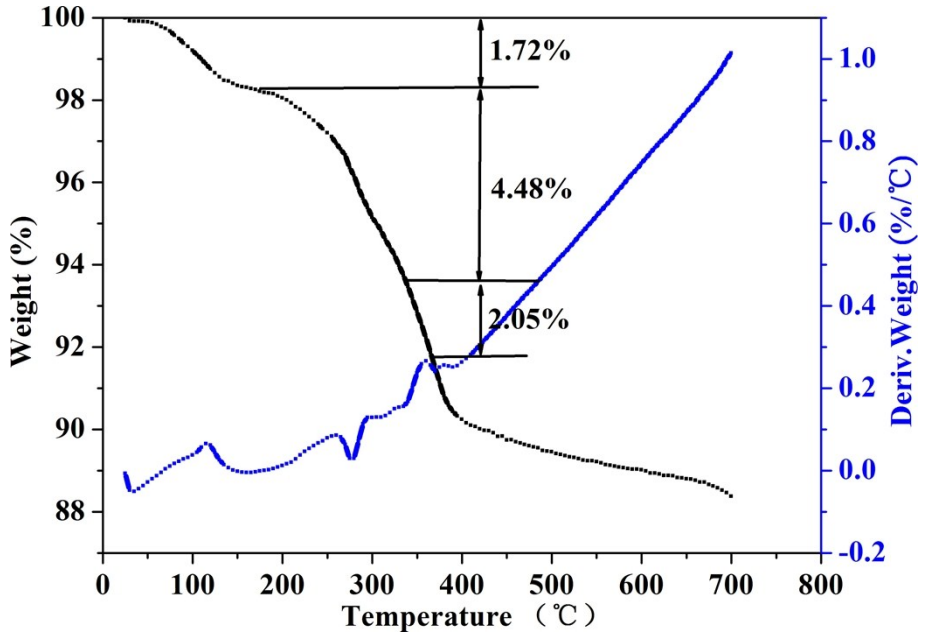

Fig. S22. TG curve of **1**. The first and second weight loss is the lost of lattice water (including isolated, binding and coordinate water molecules). Then the loss of all $\{C_2H_8N\}$ organic cations and the structure begins to decompose.

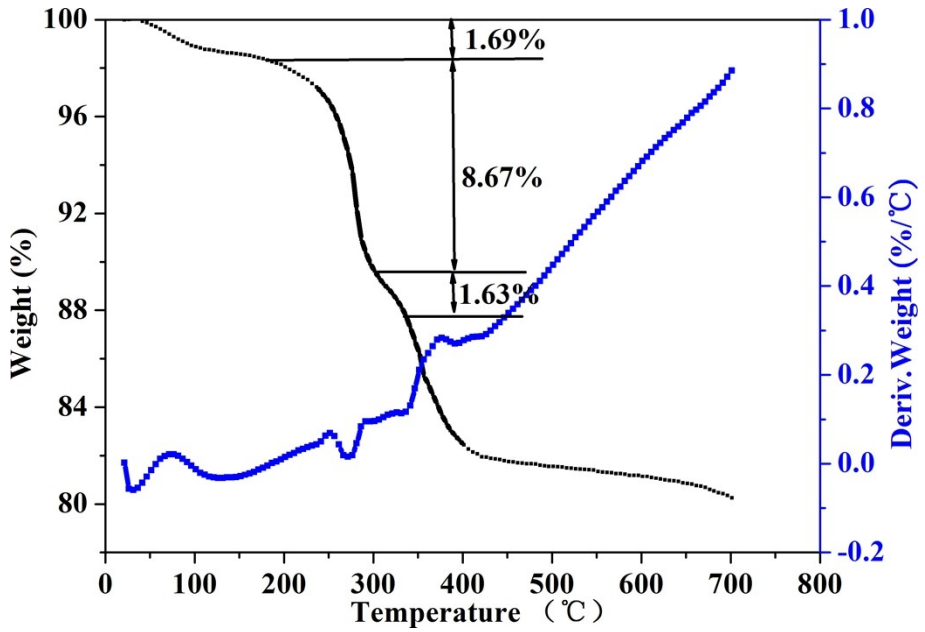

Fig. S23. TG curve of **2**. The first and second weight loss is the lost of lattice water (including isolated, binding and coordinate water molecules). Then the loss of all $\{C_2H_8N\}$ organic cations and the structure begins to decompose.